ACS Catalysis

Article

Visible Light Gold Nanocluster Photocatalyst: Selective Aerobic Oxidation of Amines to Imines

Haijun Chen, Chao Liu, Min Wang, Chaofeng Zhang, Nengchao Luo, Yehong Wang, Hadi Abroshan, Gao Li, and Feng Wang

ACS Catal., **Just Accepted Manuscript** • DOI: 10.1021/acscatal.6b03509 • Publication Date (Web): 10 Apr 2017

Just Accepted

ACS Publications

ACS Catalysis is published by the American Chemical Society. 1155 Sixteenth Street N.W., Washington, DC 20036

Visible Light Gold Nanocluster Photocatalyst: Selective Aerobic Oxidation of Amines to Imines

Haijun Chen,[a, c] Chao Liu,[b] Min Wang[a], Chaofeng Zhang[a], Nengchao Luo[a], Yehong Wang[a], Hadi Abroshan[d], Gao Li[b,*], Feng Wang[a,*]

[a] State Key Laboratory of Catalysis, Dalian National Laboratory for Clean Energy, Dalian Institute of Chemical Physics, Chinese Academy of Sciences, Dalian 116023, People's Republic of China

[b] Gold Catalysis Research Centre, State Key Laboratory of Catalysis, Dalian Institute of Chemical Physics, Chinese Academy of Sciences, Dalian 116023, People's Republic of China

[c] University of Chinese Academy of Sciences, Beijing 100049, People's Republic of China

[d] Department of Chemistry, Carnegie Mellon University, Pittsburgh, PA 15213, USA

ABSTRACT: This work demonstrates the synthesis of an efficient photocatalyst, $Au_{25}(PPh_3)_{10}Cl_2(SC_3H_6SiO_3)_5/TiO_2$, for selective oxidation of amines to imines. The photocatalyst is prepared via hydrolysis of $Au_{25}(PPh_3)_{10}Cl_2[(SC_3H_6Si(OC_2H_5)_3]_5$ nanoclusters in the presence of P25 support. The gold nanoclusters exhibit good

photocatalytic activity using visible light and under mild thermal conditions for the selective oxidation with molecular oxygen (O_2). The turnover frequency (TOF) of 4-methylbenzylamine oxidation is found to be 1522 h^{-1}, which is considerably higher than that conventional gold catalysts. The gold nanoclusters present good recyclability and stability for the oxidation of a wide range of amines. The superior activity of the photocatalyst is associated with its unique electronic structure and framework. The catalytically active sites are deemed to be the exposed gold atoms upon detaching protecting ligands, i.e., PPh_3. The Hammett parameter suggests that the photocatalytic process involves the formation of carbocation intermediate species. Further, Au-H species were confirmed by TEMPO (2,2,6,6-tetramethylpiperidinyloxy) as a trapping agent.

KEYWORDS: Gold nanoclusters, Au_{25}, photocatalysis, selective organic transformation, benzylamine oxidation

1. INTRODUCTION

Atomically precise gold nanoclusters have recently emerged as novel promising catalysts owing to their unique molecular and electronic configurations.[1] The nanoclusters display intrinsically different catalytic properties in comparison with the conventional (bare) gold nanoparticles.[2] The chemical nature of the nanoclusters often result in superior or new properties for catalytic reactions, including oxidation, hydrogenation and carbon-carbon bond formation reactions.[3] Because of their

nanometric size, the gold nanoclusters usually exhibit a non-metallic behavior with energy quantization manifested in their HOMO–LUMO gap, opposite to localized surface plasmon resonance (LSPR) of the conventional nanoparticles.[2b] The electrons of the gold nanoclusters can be excited from HOMO to LUMO upon illumination, resulting in the formation of electron-hole pairs just as semiconductors do.[4] The generation and subsequent recombination of the electron–hole pairs using solar energy are of great interest for photocatalytic and photovoltaics applications. For example, the catalytic activity of gold nanoclusters have been demonstrated in solar energy harvesting for power generation, pollutant degradation, and hydrogen production.[4b, 5]

Among gold nanoclusters, $Au_{25}(PPh_3)_{10}(SR)_5Cl_2$ nanoclusters, here "-SR" representing thiolate ligand, show a distinct absorption spectrum in the visible region.[6] This nanocluster with a HOMO-LUMO gap of 1.9 eV and a unique framework helping phosphine ligand dynamically opens up an exciting possibility for practical applications in solar energy harvesting.[7] Light-induced electrons with large reduction potentials can easily activate O_2 to mediate energy, thus facilitating oxidation reactions. Using emission spectra and photocurrent experiments, Kamat et al. showed that the electrons of gold clusters excited by visible light can be injected into the conduction band of TiO_2 (cluster's support).[8] The $Au_{25}(PPh_3)_{10}(SR)_5Cl_2$ nanocluster can absorb light, leading to the separation of electrons and holes. The excited electrons would later be injected into the supports (e.g., P25) because the LUMO energy of Au_{25} cluster (-0.63 V)[9] is higher than the conduction edge (-0.09 V) of P25.[10]

Selective oxidation of amines to imines is of significant importance due to the versatile applications of the product (imines) in fine chemicals and pharmaceuticals.[11] Tada and coworkers developed a plasmonic gold photocatalyst which gave 4.5% conversion of benzylamine to imine in the absence of solvent.[12] Herein, we investigate the photocatalytic performance of the P25-supported $Au_{25}(PPh_3)_{10}(SC_3H_6SiO_3)_5Cl_2$ nanoclusters in the selective oxidation of amines to imines with O_2 under mild conditions (ca. 30 ºC). A TOF of 1522 h^{-1} obtained on this gold nanocluster photocatalyst is much higher than the conventional gold nanoparticles. To our knowledge, there have been few reports so far regarding the photocatalytically selective oxidation of organic compounds by well-defined Au clusters except in the oxidation of sulfides.[13]

2. EXPERIMENTAL SECTION

Synthesis of $Au_{25}Cl_2(PPh_3)_{10}(SC_3H_6SiO_3)_5$/P25 Photocatalyst

Seventy six mg of $Au(PPh_3)Cl$ and 76 μL of MPTES was dissolved in a mixed solution (5 mL of CH_2Cl_2 and 5 mL of ethanol) under ultrasonic condition, followed by stirring for 20 min. Then, 6 mg of $NaBH_4$ dispersed in 2 mL of ethanol was added dropwise. After 30 min of reaction, 38 μL of MPTES was injected into the system. The reaction was terminated when the absorption features of Au_{25} clusters appeared in the UV-vis spectrum of the solution. The solvent was evaporated by rotary evaporation. The $Au_{25}(PPh_3)_{10}[SC_3H_6Si(OC_2H_5)_3]_5Cl_2$ nanoclusters were obtained by extraction with acetonitrile. And then redissolved in 9 mL of chloromethane. About 6 mL of the cluster solution was diluted with 24 mL of dichloromethane, and then 1 g of P25 was added.

After stirring for 12 h, the obtained solids were collected by centrifugation and washed by dichloromethane three times. The $Au_{25}(PPh_3)_{10}Cl_2[SC_3H_6SiO_3]_5$/P25 solids were dried in vacuum at 60 ℃, and denoted hereafter as [Au_{25}]/P25. The synthesis of anatase and rutile supported $Au_{25}(PPh_3)_{10}Cl_2(SR)_5$ (R= $SC_3H_6SiO_3$) nanoclusters followed almost the same procedure, except P25 was replaced by anatase and rutile (denoted here after as [Au_{25}]/A-TiO_2 and [Au25]/R-TiO_2).

Synthesis of AuNP/P25

0.2 g of P25 impregnated with CH_3OH was dispersed in 50 mL of H_2O, 0.2 mL of $HAuCl_4$ (24.3 mM) was added with stirring for 10 min. Then the suspension was irradiated under high-voltage mercury lamp for 30 min. The obtained solid was washed with water and dried in vacuum at 60 ℃ for 10 h. Then, AuNP/P25 was obtained.

Photocatalytic Oxidation of Amines

In a typical oxidation reaction, 2 mg of photocatalyst was placed in a 5 mL quartz tube with a magnetic stirrer. The system was first furnished with O_2. This followed by addition 0.2 mmol of benzylamine, 0.1 mmol of *p*-xylene, 1 mL of CH_3CN. The tube was sealed and irradiated with a 9.6 W LED light (455 nm). After the reaction, the catalysts were separated by a membrane filter. The remaining liquid was examined by GC and GC-MS. The conversion and selectivity were determined using internal standard method.

Characterization

The UV-vis spectra were acquired on a Hewlett-Packard Agilent 8453 diode array spectrophotometer at room temperature. Diffuse reflectance UV-vis spectra were recorded by PerkinElmer Lamada 750 UV/VIS/NIR Spectrometer. FTIR spectra were collected on a Bruker Tensor 27 instrument. The transmission electron microscopy (TEM) was performed on a JEM-2100 microscope at an accelerating voltage of 200 kV. Solid state ^{31}P magic-angle-spinning (MAS) NMR experiment was conducted in a Bruker Avance III 500 MHz NMR spectrometer equipped with a 4 mm standard bore probe head, using a magnetic field of 11.7 T at 300 K. The sample was packed in the ZrO_2 rotor closed with Kel-F cap, which was then spun at 8 kHz rate. A total of 5000 scans were recorded with 5 s recycle delay for each sample. ^{31}P MAS chemical shift is referenced to the resonances of ADP standard (δ=0.81 ppm). Ultrahigh resolution mass spectrum was acquired using a Bruker SolariX FT-ICR-MS equipped with a 15.0 T superconducting magnet and an ESI ion source. Sample for ESI FT-ICR-MS analysis was continuously infused into the ESI unit by syringe infusion at a flow rate of 120 μL h^{-1}. The ESI needle voltage was set to 4.5 kV. The samples was analyzed in positive ionization mode with broadband detection. Ions accumulated in a hexapol ion trap for 0.2 s before being introduced into the ICR cell. 4 M words of data were recorded per broadband mass scan. The lower mass limit was set to m/z = 152.45 Da and the upper mass limit to m/z = 10000 Da. The concentration of gold was determined by inductively coupled plasma-atomic emission spectrometry (ICP-AES; ICPS-8100, Shimadzu). The specific surface area of P25 (72.9 m^2 g^{-1}) was measured by Micromeritics ASAP 2020 surface area analyzer (Quantachrome). The apparent quantum efficiency (AQE)

measurement was carried out using a Pyrex top-irradiation-type reaction vessel and a 300 W xenon lamp fitted with a filter. The number of photons reaching the reaction solution was measured using a calibrated Si photodiode (LS-100, EKO Instruments Co., LTD.), and the AQE was calculated according to the following equation:

$$\text{AQE} = \frac{\text{amounts of products formed}}{\text{amounts of photons irradiated}}$$

We consider one absorbed photons will produce one product. All the AQE measurements were based on a product yield of less than 20%.

Computational details.

Geometry optimization of $Au_{25}(PH_3)_{10}(SH)_5$ as a model of the nanocluster was performed using the Gaussian09 package with the B3PW91 hybrid density functional. The 6-31G** basis set was employed for H, P, S and Cl.[14] The LANL2DZ basis set was used for gold atoms.[15] The energy required for removal of a ligand from the nanocluster is estimated as the energy difference $\Delta E = E(\text{NC-L}) + E(\text{L}) - E(\text{NC})$, where E(NC), E(NC-L), and E(L) are total energies of the isolated nanocluster, the nanocluster with one ligand removed, and the ligand, respectively. The integral equation formalism polarizable continuum model (IEFPCM) was applied to account for the solvation effect.[16]

3. RESULTS AND DISCUSSION

3.1 Synthesis and Characterization of [Au_{25}]/P25 Catalysts.

The $Au_{25}(PPh_3)_{10}[SC_3H_6Si(OC_2H_5)_3]_5Cl_2$ nanocluster was synthesized via a one-phase size-focusing method. In a typical procedure, the gold nanoclusters were prepared

through a simple reduction of $Au(PPh_3)Cl$ with sodium borohydride in the presence of excess MPTES (3-mercaptopropyltriethoxysilane). The final products were obtained by centrifugation and purification. The yield of the obtained Au_{25} nanocluster was ~ 52% based on the $Au(PPh_3)Cl$ consumption.

The as-syhtnesized gold nanoclusters were firstly characterized by ultraviolet–visible spectroscopy (UV-vis). As shown in Figure 1a, red line, the distinct absorption peaks of the free $Au_{25}(PPh_3)_{10}(SC_3H_6Si(OC_2H_5)_3)_5Cl_2$ nanoclusters (dispersed in ethanol) appeared at 415, 445 and 675 nm, consistent with reportedly neat $Au_{25}(PPh_3)_{10}(SR)_5Cl_2$ nanoclusters in literatures (Figure S1).[6, 17] This is different from the local surface plasmon resonance (LSPR) effect of Au nanoparticle (AuNP) supported P25 (Figure 1a, green line). For addtional insights, we performed TD-DFT calculations of $[Au_{25}(PH_3)_{10}Cl_2(SH)_5]^{2+}$, as a model of the nanocluster (Figure S2). Results indicated that the first peak at 675 nm (1.84 eV) is attributed to HOMO–LUMO excitation of the $Au_{25}(PPh_3)_{10}(SR)_5Cl_2$ nanoclusters. The other absorption peaks and shoulder are found to correspond to the mixtures of electronic transition of HOMO-*m* → LUMO+*n*, which *m* and *n* are positive integer. To determine the exact composition of the gold nanoclusters, Fourier transform-ion cyclotron resonance-mass spectrometry (FT-ICR-MS) with the ESI soft ionization technique was employed, as it usually does not lead to cluster fragmentation.[18] The mass signal was centered at m/z = 4402.2 (where z = 2, Figure S3), corresponding to the doubly charged $[Au_{25}(PPh_3)_{10}(SC_3H_6Si(OC_2H_5)_3)_5Cl_2]^{2+}$ (theoretical value m/z = 4402.5, deviation: ± 0.3). The TEM image showed that the size of the metal core of the free standing gold

nanoclusters is ~ 1.2 nm (Figure 1b), matching well with the framework of $Au_{25}(PPh_3)_{10}(SR)_5Cl_2$.[3e, 3j]

Next, the $Au_{25}(PPh_3)_{10}Cl_2(SC_3H_6SiO_3)_5$/P25 photocatalyst (denoted as [Au_{25}]/P25, hereafter) was obtained via a hydrolysis process of $Au_{25}(PPh_3)_{10}Cl_2(SC_3H_6Si(OC_2H_5)_3)_5$ nanoclusters with hydroxyl group of P25. Of note, the P25 nanocrystals comprise two phases, anatase and rutile.[4b] The diffuse reflectance UV-vis spectrum of [Au_{25}]/P25 showed similar optical peaks (especially the characteristic peak at 675 nm) with that of the unsupported nanoclusters (Figure 1a blue line vs. red line), implying that the [Au_{25}] nanoclusters keep intact on the P25 surface. FT-IR analysis indicated that both the phosphine and thiolate ligands ligate on the nanoclusters (Figure S4). Further, the [Au_{25}]/P25 catalysts were analyzed by solid state ^{31}P magic angle spinning (MAS) NMR spectroscopy (Figure 1c). Only one single peak at δ = 33.2 ppm was observed in the NMR analysis, indicating that the PPh_3 ligands are bonded with the gold atoms.[19] Furthermore, TEM analysis showed that the [Au_{25}] is immobilized on the P25 surface and the diameter of cluster is still ~1.2 nm (Figure 1d and S5), which is same as that of the unsupported clusters, also suggesting that the [Au_{25}] nanocluster remains intact on the P25 surface. Of note, the ICP analysis showed that the gold content of the [Au_{25}]/P25 was ~ 1.04 wt%. Next, the as-prepared [Au_{25}]/P25 was investigated in the aerobic photocatalytic oxidation of amines to imines without any other pretreatments.

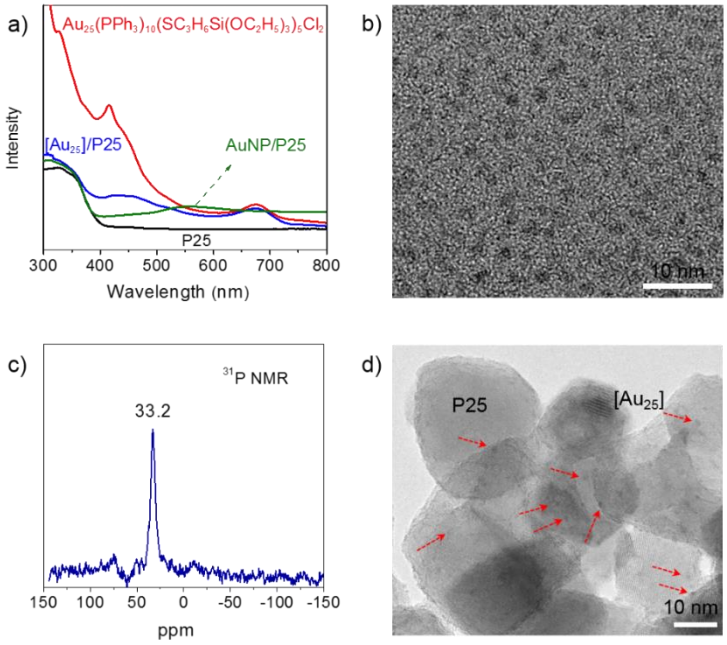

Figure 1. a) UV-vis of $Au_{25}(PPh_3)_{10}(SC_3H_6Si(OC_2H_5)_3)_5Cl_2$ nanoclusters (dispersed in ethanol), and diffuse reflectance UV-vis spectra of the [Au_{25}]/P25 photocatalyst, AuNP/P25 and P25 support. b) TEM image of $Au_{25}(PPh_3)_{10}(SC_3H_6Si(OC_2H_5)_3)_5Cl_2$. c) Solid state ^{31}P MAS NMR spectrum of the [Au_{25}]/P25. d) TEM image of the [Au_{25}]/P25.

3.2 Photocatalytic Properties of [Au_{25}]/P25

In the previous literatures, the TiO_2 oxides exhibited some activity in the aerobic photocatalytic oxidation of benzylamine via a surface complex mechanism.[20] Therefore, we firstly investigated and compared the catalytic performance of three different TiO_2 semiconductors (P25, A-TiO_2, and R-TiO_2; A represents anatase and R rutile) and the corresponding TiO_2-supported gold nanocluster catalysts ([Au_{25}]/P25, [Au_{25}]/A-TiO_2, and [Au_{25}]/R-TiO_2) in the photocatalytic oxidation of benzylamine. The photocatalysis was carried out under the conditions as indicated in Table 1. About 12-16%

benzylamine conversion with ≥ 99% selectivity for imine was achieved when using P25, A-TiO_2 and R-TiO_2 as the catalysts (Table 1, entries 4-6), while the [Au_{25}] catalysts, supported on the TiO_2 showed much better catalytic activity under the identical reaction conditions. The conversion was improved to 45% for [Au_{25}]/R-TiO_2, 67% for [Au_{25}]/A-TiO_2, and 80% for [Au_{25}]/P25. In all cases, the selectivity was above 99% (Table 1, entries 1-3). In a control experiment without TiO_2 and the gold cluster, no activity was observed at all (Table 1, entry 7). The [Au_{25}]/P25 catalyst showed no activity in the absence of light irradiation and only 3% conversion under Ar atmosphere (Table 1, entries 8 and 9). Thus, it indicates that the photocatalysis is indeed promoted by oxygen and is associated with the nanoclusters.

Table 1. Catalytic performance of various catalysts in the photo-oxidation of benzylamine.[a]

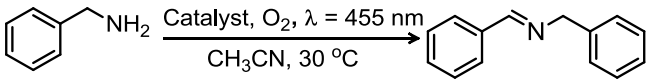

entry	catalyst	conv. (%)[b]	sel. (%)[b]
1	[Au_{25}]/A-TiO_2	67	99
2	[Au_{25}]/R-TiO_2	45	99
3	[Au_{25}]/P25	80	99
4	P25	14	99
5	A-TiO_2	16	99
6	R-TiO_2	12	99
7	–	0	–
8[c, e]	[Au_{25}]/P25	0	–
9[d, e]	[Au_{25}]/P25	3	99
10	AuNP/P25	14	99
11	[Au_{25}]/P25-300[f]	14	99

[a]Reaction conditions: 2 mg of catalyst, 0.2 mmol of benzylamine, 1 mL of CH_3CN, 0.1 mmol of *p*-xylene as internal standard, O_2 1 atm, 455 nm light, 2 h. [b]The conversion (conv.) and selectivity (sel.) for imines are determined by GC. [c]In absence of light, 40 ℃. [d]Protected by Ar. [e]10 mg catalyst, 1.5 h. [f]Annealed at 300 ℃ for 4 h in a H_2 atmosphere.

Next, for the purpose of control, we prepared a P25-supported gold nanoparticle (AuNP/P25) by photoreduction method. The average size of gold NP was ~ 2.0 nm (Figure S6). Surprisingly, the AuNP/P25 catalyst only gave 14% conversion (entry

10), which was close to the pure P25 catalyst under the same reaction conditions. The [Au_{25}]/P25 catalyst, annealed at 300 ℃ for 4 h and noted as [Au_{25}]/P25-300, showed low catalytic activity (14% conversion) similar to that of the AuNP/P25 catalyst (Table 1, entry 11). Of note, after the heat treatment, the structure of [Au_{25}] nanoclusters was destroyed and only LSPR effect was showed in Figure S7. Further, we measured the action spectra of [Au_{25}]/P25, which show that the apparent quantum efficiency at different irradiation wavelengths were in agreement with the absorption of [Au_{25}]/P25 (Figure S8). These results may indicate the reaction was photocatalyzed by the excitation of gold cluster. We also measured the average AQE using the wavelength range from 500 to 800 nm and a result of 4.7% (5.2% at 460 nm) was obtained. These results indicate the photo-excited electrons of gold cluster were facilitated to the oxidation because the complex between surface hydroxyl of TiO_2 and benzylamine scarcely absorb light longer than 500 nm.[20] Consequently, the distinct LSPR effect of AuNP (Figure 1, green line) and surface complex mechanism cannot attribute to the photocatalytic oxidation reaction, indicating that the photocatalyzed oxidation is mainly induced by [Au_{25}] cluster with suitable electronic property and structure.

Further, the reaction kinetics of [Au_{25}]/P25 and P25 catalysts were studied by monitoring the conversion of benzylamine at different time interval. It was found that > 50% benzylamine was converted within 90 min when the reaction was catalyzed by [Au_{25}]/P25 catalyst, while plain P25 merely gave a 7% conversion, as depicted in Figure 2. After an irradiation time for 2 h, the benzylamine conversion

reached up to 82% for [Au_{25}]/P25 and 14% for P25. The superior catalytic activity of [Au_{25}]/P25 than pure P25 indicates a different reaction pathway, discussed *vide infra*. The TOF of the [Au_{25}]/P25 photocatalyst (TOF = (reacted mol of amine)/[(mol of Au atoms) ×reaction time in hour)]) was calculated to be 878 h^{-1} based on a benzylamine conversion of 14%, which is much higher than those catalyzed by AuNP and other metals (Table S1).

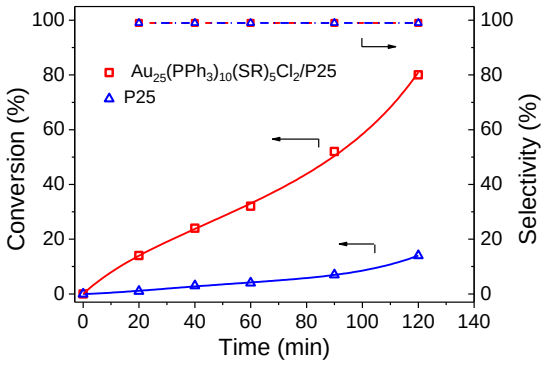

Figure 2. Time-dependent catalytic performances of [Au_{25}]/P25 and P25 in the photocatalyzed oxidation of benzylamine. (Reaction conditions: 2 mg of catalyst, 0.2 mmol of benzylamine, 1 mL of CH_3CN, 0.1 mmol of *p*-xylene as internal standard, O_2 1 atm, ~30 ℃, 455 nm LED).

The catalytic activity of [Au_{25}]/P25 was further examined with various amines derivatives. As shown in Table 2, both the benzylamines with electron-withdrawing and electron-donating groups gave good conversions (73–99%), excellent selectivity to corresponding imines (Table 2, entries 2-6). The 2-bromobenzylamine was relatively inert to be converted (73% conversion, Table 2, entry 4), which reveals the presence of

steric effect. Heterocyclic amine containing of sulfur could also be oxidized to the corresponding imine in excellent yield (Table 2, entry 7), albeit the sulfur species usually poison metal catalysts. Over-oxidation occurred which resulted in a methylene decreased in the final product for phenylethylamine oxidation; a conversion of 69% with a selectivity of 87% to 1-phenyl-*N*-(2-phenylethylidene)methanamine was obtained (Table 2, entry 8), consistent with the previous results.[21] It is worthy to note that the TOF was calculated to be 1522 h^{-1} based on the 4-methylbenzlamine conversion of 26%. Furthermore, we conducted the catalyst recyclability for the benzylamine photocatalytic oxidation. Only <10% decreasing activity was observed after three cycles all with the selectivity more than 99% (Figure 3).

Table 2. Photocatalytic oxidation of a range of amine substrates over [Au_{25}]/P25 catalyst.[a]

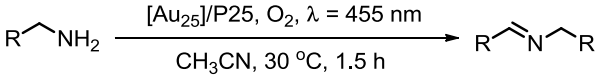

entry	substrate	product	conv. (%)	sel. (%)	TOF(h^{-1})[d]
1	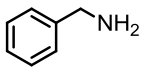	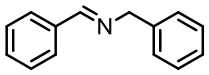	98	99	878
2	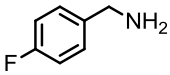	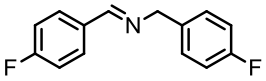	82	99	1049
3	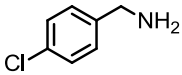	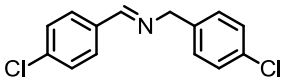	97	99	1184
4	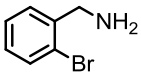	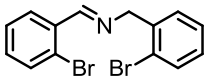	73	97	312[e]
5	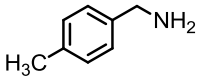	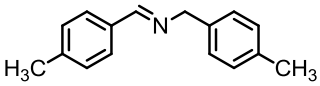	99	99	1522
6[b]	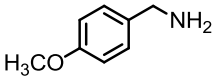	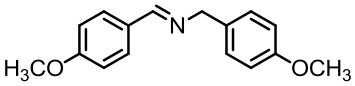	96	97	1025
7[c]	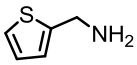	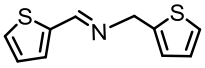	94	99	638[e]
8[c]	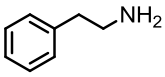	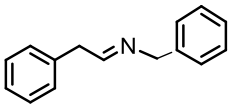	69	87	

[a]Reaction conditions: 10 mg of catalyst, 0.2 mmol of benzylamine, 1 mL of CH_3CN, 0.1 mmol of *p*-xylene as internal standard, O_2 1 atm, 455 nm LED, 1.5 h. [b]2 h, [c]3 h. [d]TOF was calculated based on reaction for 20 min using 2 mg catalyst, conversion between 13-26%. [e]30min.

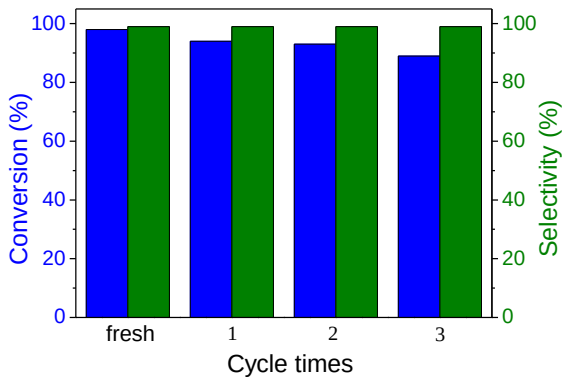

Figure 3. Cycling tests of benzylamine oxidation catalyzed by [Au_{25}]/P25.

3.3 Photocatalytic Mechanism Investigation

To get more insight into the role of photo-generated radical species in these photocatalytic redox reactions, the controlled experiments were conducted. Figure 4 showed the effect of different radical scavengers over photocatalytic oxidation of benzylamine under visible light. Significant decreasing activities for the photocatalysis were observed when $K_2S_2O_8$ (scavenger for electrons[22]) and ammonium oxalate (AO, scavenger for holes[23]) were added into the photocatalysis system. These results clearly demonstrate that both photo-generated holes and electrons are initial drivers for the photocatalytic reactions. The [Au_{25}] nanoclusters supported on P25 absorbing the light can act as a narrow band gap semiconductor leading to separation of electrons and holes.[4b] The electrons can be injected into the conduction band of P25, thus enhancing the separation efficiency of electrons and holes.[4c, 24] The more efficient separation of carriers can facilitate the oxidation reaction. A reasonably near linearity relationship

between log(k_X/k_H) and the Brown-Okamoto constant σ was established for the oxidation of *para*-substituted benzylamine (F, Cl, H, CH_3, OCH_3) as shown in Figure S10. The slop of the plot (ρ value) is negative, indicating that the reaction is probably via carbocation intermediate species.

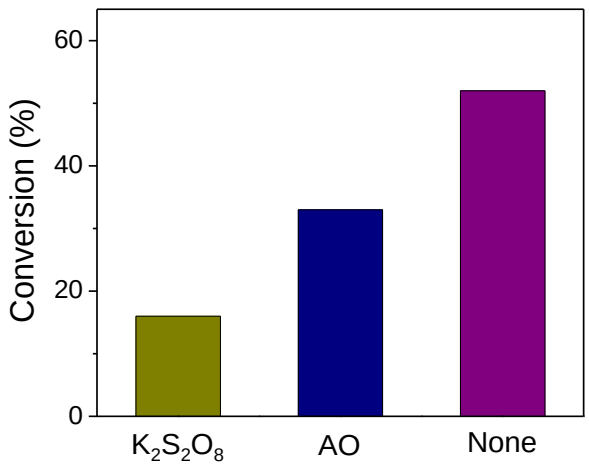

Figure 4. Controlled experiments using different radical scavengers for the photocatalytic selective oxidation of benzylamine over [Au_{25}]/P25. AO= ammonium oxalate.

Table 3. Photocatalytic amine oxidation over various catalysts.[a]

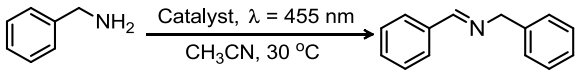

entry	catalyst	additive	conv. (%)	sel. (%)
1	$[Au_{25}]$/P25	–	98	99
2	$Au_{25}(SC_2H_4Ph)_{18}$/P25	–	33	99
3	AuNP/P25	PPh_3[b]	53	95
4	$Au_{11}(PPh_3)_7Cl_3$/P25	–	85	99
5	$Au_{101}(PPh_3)_{21}Cl_5$/P25	–	44	99
6	$[Au_{25}]Cl_2$/P25	TEMPO[c]	20	99
7	–	TEMPO[c]	2	99

[a]Reaction conditions: 10 mg of catalyst, 0.2 mmol of benzylamine, 1 mL of CH_3CN, 0.1 mmol of *p*-xylene as internal standard, O_2 1 atm, 455 nm LED, 1.5 h.[b]n_{PPh_3}:n_{Au}=27.6, [c]0.4 mmol of TEMPO ,under Ar.

Next, for comparison, we prepared a $Au_{25}(SC_2H_4Ph)_{18}$/P25 catalyst (Figure S11).[3j, 25] Intriguingly, the $Au_{25}(SC_2H_4Ph)_{18}$/P25 showed a very low catalytic activity (Table 3, entry 2). On the other hand, the AuNP/P25 catalyst exhibited no increase in catalytic activity in the presence of excess PPh_3 (Table 3, entry 3), suggesting that the PPh_3 cannot influence the catalytic activity. Therefore, the electronic property and

framework of [Au_{25}] nanocluster should account for the high catalytic activity. Further, the $Au_{11}(PPh_3)_7Cl_3$ and $Au_{101}(PPh_3)_{21}Cl_5$ nanoclusters were synthesized using protocols presented in previous studies (Figure S12).[26] The $Au_{11}(PPh_3)_7Cl_3$/P25 and $Au_{101}(PPh_3)_{21}Cl_5$/P25 catalysts gave conversion of 85% and 44%, respectively (Table 3, entries 4 and 5) in the benzylamine photocatalytic oxidation, which are considerably lower than that for P25-supported [Au_{25}] (98%). It is also worth noting that no direct size dependence of the cluster catalyst was observed. Further, we conducted the photocatalysis of benzylamine over [Au_{25}]/P25 using TEMPO to abstract hydrogen under Ar atmosphere. It is pointed out that TEMPO can abstract hydrogen from the metal surface instead of from the substrate, which plays a similar role as oxygen.[27] A 20% conversion was obtained when TEMPO was present without oxygen (Table 3, entry 6). Of note, TEMPO itself (without cluster catalyst) cannot oxidize benzylamine, demonstrating that the Au-H species were indeed generated during the photocatalytic reaction.

Table 4. DFT results on the energy (eV) required for the removal a ligand from $[Au_{25}(PH_3)_{10}(SH)_5Cl_2]^{2+}$ cluster as a model of the nanocluster in gas and solution (acetonitrile) phases.

	PH_3	-SH	-Cl
Gas phase	1.2	10.1	8.2
Solution phase	1.3	2.7	0.9

Then, we briefly discuss the possible mechanism for the photocatalytic reaction over the gold nanocluster. The [Au_{25}] clusters are comprised of two biicosahedral Au_{13} units which are surrounded by PPh_3 and MPTES ligands (Figure S13). The DFT

simulations suggest that the benzylamine reactant cannot be adsorbed on the surface of gold clusters. Therefore, we initially speculated that there should be partial ligand removal under the reaction conditions, providing active sites for the oxidation. Our previous studies have found that the phosphine ligands on the gold nanoclusters (e.g., $[Au_{11}(PPh_3)_7Cl_3]^+$ and $[Au_{25}(C{\equiv}CPh)_5(PPh_3)_{10}Cl_2]^{2+}$ clusters) can be partially detached in the presence of amine (e.g., NH_3), strongly evidenced by the experiments and theoretical calculations.[28] Three organic ligands (i.e., PPh_3, MPTES, and Cl) are ligated on the gold nanoclusters and can be lost during the catalytic process. We here choose $[Au_{25}(PH_3)_{10}(SH)_5Cl_2]^{2+}$ as a model for the simulations to rationalize the possible ligand removal process in the presence of amine. Table 4 showed the energy (eV) required for removing a ligand of different types from $[Au_{25}(PH_3)_{10}(SH)_5Cl_2]^{2+}$ nanocluster in gas and solution (acetonitrile, using polarizable continuum model) phases. Results indicated the detachment of a Cl^- or PH_3 ligands required 0.9 and 1.3 eV/mol, respectively, which are considerably lower than that for removing a thiolate ligand (2.7 eV/mol). These results indicate Cl^- and phosphine ligands have higher potentials to leave the nanoclusters, thereby providing gold open metal sites. We think that the removal of a phosphine ligand is more favorable than Cl^- in solution phase, especially due to the high charge density of $[Au_{25}]^{3+}$ formed upon removal of a Cl^-. This may not be captured in DFT calculations since we replaced PPh_3 with PH_3 in our model as well as overestimation of the solvation effect by continuum approach.

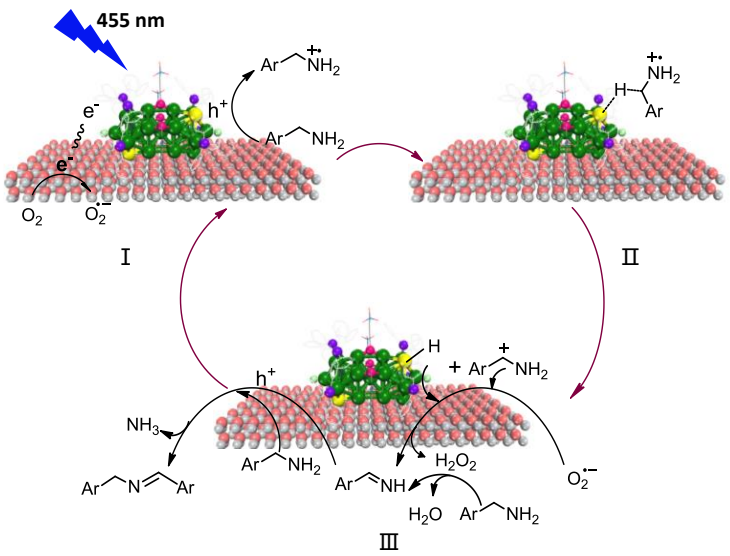

Scheme 1. Proposed mechanism for photo-oxidation of benzylamine catalyzed by TiO_2-suppported [Au_{25}] clusters. Color codes: Au, green; exposed Au, yellow; P, purple; S, magenta; Cl, light green; Ti, gray; O, pink. Partial carbon and hydrogen atoms are omitted for clarity.

Finally, the reaction mechanism can be rationalized as follows (Scheme 1). [Au_{25}] cluster absorbs light which leads to separation of electrons and holes. The excited electron is injected into the P25 support, and O_2 is reduced to $O_2^{\bullet-}$ species (Scheme S1). This has been already confirmed by electron spin resonance in a preceding work.[29] The holes can abstract an electron from the benzylamine to yield a benzylamine radical cation, which was also reported previously.[30] and then the α-H of benzylamine radical cation can be abstracted by the exposed gold atom on the nanocluster surface, and then an Au-H intermediate is formed accompanied by producing a carbocation intermediate. Next, the $O_2^{\bullet-}$ species would abstract H from the Au-H and the amine to produce Ph-CH=NH and H_2O_2 (Scheme S1). H_2O_2 was detected by the $KMnO_4$ as shown in Figure

S14. Further, if H_2O_2 was used as oxidant, the reaction proceeded more quickly than using O_2 as oxidant (Figure S15), also indicating peroxide species may be the active intermediate. The H_2O_2 would be soon decomposed by oxiding benzyalamine that give water and benzaldimine.[30b] notably, the Ph-CH=NH intermediates are very active in the photocatalysis reaction of benzylamine.[12, 30a]. The benzaldimine is subjected to nucleophilic attack by benzylamine to form aminal.[30b] Finally, the aminal group can eliminate the ammonia to afford the imine product.

4. CONCLUSION

In summary, we have synthesized atomically precise $Au_{25}(PPh_3)_{10}[SC_3H_6Si(OC_2H_5)_3]_5Cl_2$ nanoclusters supported on P25 exhibiting superior selective visible light photocatalytic oxidation of amines to imines with molecular oxygen. The high catalytic activity arises from the photo-excited separation of electrons and holes of the $Au_{25}(PPh_3)_{10}(SR)_5Cl_2$ nanoclusters instead of the LSPR effect. The turnover frequency reaches up to 1522 h^{-1} in the 4-methylbenzylamine oxidation. The catalytic active sites are the exposed gold atoms due to the partial removal of PPh_3 ligand. The photocatalysis proceeds a carbocation intermediate and Au-H intermediate species. This work may lay a firm foundation of visible light photocatalytic selective organic transformation over gold nanoclusters.

ASSOCIATED CONTENT

Supporting Information.

The Supporting information is free of charge on the ACS Publications website at xxx.

Additional characterization data, including Uv-vis, FT-ICR-MS and IR spectra, TEM image, Diffuse reflectance UV-vis spectroscopy, details regarding data processing, kinetics data, Au_{25} schematic drawing(PDF).

AUTHOR INFORMATION

Corresponding Authors

*Tel. / Fax: (+86) 0411-84379762. E-mail: wangfeng@dicp.ac.cn (F. Wang)

*Tel / Fax: (+86) 0411-82463017. E-mail: gaoli@dicp.ac.cn (G. Li)

Author Contributions

The manuscript was written through contributions of all authors. All authors have given approval to the final version of the manuscript.

ORCID

Feng Wang: 0000-0002-9167-8743

Notes

The authors declare no competing financial interest.

ACKNOWLEDGMENT

We thank the National Natural Science Foundation of China (21422308, 21690080 and 21601178), the Strategic Priority Research Program of CAS

(XDB17020300) and the starting funds of "Thousand Youth Talents Plan" (GL) for financial support.

REFERENCES

1. Jin, R.; Zeng, C.; Zhou, M.; Chen, Y. *Chem. Rev.* **2016,** *116,* 10346-10413.

2. (a) Li, G.; Jin, R. *Acc. Chem. Res.* **2013,** *46,* 1749-1758; (b) Yamazoe, S.; Koyasu, K.; Tsukuda, T. *Acc. Chem. Res.* **2014,** *47,* 816-824.

3. (a) Fang, J.; Zhang, B.; Yao, Q.; Yang, Y.; Xie, J.; Yan, N. *Coord. Chem. Rev.* **2016,** *322,* 1-29; (b) Lopez-Acevedo, O.; Kacprzak, K. A.; Akola, J.; Hakkinen, H. *Nat. Chem.* **2010,** *2,* 329-334; (c) Lee, S.; Molina, L. M.; Lopez, M. J.; Alonso, J. A.; Hammer, B.; Lee, B.; Seifert, S.; Winans, R. E.; Elam, J. W.; Pellin, M. J.; Vajda, S. *Angew Chem. Int. Ed.* **2009,** *48,* 1467-1471; (d) Liu, Y.; Tsunoyama, H.; Akita, T.; Xie, S.; Tsukuda, T. *ACS Catal.* **2011,** *1,* 2-6; (e) Wu, Z. l.; Jiang, D.-e.; Mann, A. K. P.; Mullins, D. R.; Qiao, Z.; Allard, L. F.; Zeng, C.; Jin, R. c.; Overbury, S. H. *J. Am. Chem. Soc.* **2014,** *136,* 6111-6122; (f) Yoskamtorn, T.; Yamazoe, S.; Takahata, R.; Nishigaki, J. i.; Thivasasith, A.; Limtrakul, J.; Tsukuda, T. *ACS Catal.* **2014,** *4,* 3696-3700; (g) Kauffman, D. R.; Alfonso, D.; Matranga, C.; Qian, H.; Jin, R. *J. Am. Chem. Soc.* **2012,** *134,* 10237-10243; (h) Zhu, Y.; Wu, Z.; Gayathri, C.; Qian, H.; Gil, R. R.; Jin, R. *J. Catal.* **2010,** *271,* 155-160; (i) Shivhare, A.; Ambrose, S. J.; Zhang, H.; Purves, R. W.; Scott, R. W. J. *Chem. Commun.* **2013,** *49,* 276-278; (j) Li, G.; Jin, R. *J. Am. Chem. Soc.* **2014,** *136,* 11347-11354; (k) Fang, J.; Li, J.; Zhang, B.; Yuan, X.;

Asakura, H.; Tanaka, T.; Teramura, K.; Xie, J.; Yan, N. *Nanoscale* **2015,** *7,* 6325-6333; (l) Abroshan, H.; Li, G.; Lin, J.; Kim, H. J.; Jin, R. *J. Catal.* **2016,** *337,* 72-79.

4. (a) Akimov, A. V.; Neukirch, A. J.; Prezhdo, O. V. *Chem. Rev.* **2013,** *113,* 4496-4565; (b) Yu, C. l.; Li, G.; Kumar, S.; Kawasaki, H.; Jin, R. c. *J. Phys. Chem. Lett.* **2013,** *4,* 2847-2852; (c) Chen, Y.-S.; Kamat, P. V. *J. Am. Chem. Soc.* **2014,** *136,* 6075-6082.

5. (a) Sakai, N.; Tatsuma, T. *Adv. Mater.* **2010,** *22,* 3185-3188; (b) Negishi, Y.; Matsuura, Y.; Tomizawa, R.; Kurashige, W.; Niihori, Y.; Takayama, T.; Iwase, A.; Kudo, A. *J. Phys. Chem. C* **2015,** *119,* 11224-11232; (c) Xiao, F.-X.; Hung, S.-F.; Miao, J.; Wang, H.-Y.; Yang, H.; Liu, B. *Small* **2015,** *11,* 554-567; (d) Kogo, A.; Sakai, N.; Tatsuma, T. *Electrochem. Commun.* **2010,** *12,* 996-999; (e) Liu, S.; Xu, Y. *Sci. Rep.* **2016,** *6,* 22742.

6. Shichibu, Y.; Negishi, Y.; Watanabe, T.; Chaki, N. K.; Kawaguchi, H.; Tsukuda, T. *J. Phys. Chem. C* **2007,** *111,* 7845-7847.

7. Devadas, M. S.; Thanthirige, V. D.; Bairu, S.; Sinn, E.; Ramakrishna, G. *J. Phys. Chem. C* **2013,** *117,* 23155-23161.

8. Chen, Y. S.; Choi, H.; Kamat, P. V. *J. Am. Chem. Soc.* **2013,** *135,* 8822-8825.

9. Park, S.; Lee, D. *Langmuir* **2012,** *28,* 7049-7054.

10. Leung, D. Y.; Fu, X.; Wang, C.; Ni, M.; Leung, M. K.; Wang, X.; Fu, X. *ChemSusChem* **2010,** *3,* 681-694.

11. (a) Murahashi, S. I. *Angew. Chem. Int. Ed.* **1995,** *34,* 2443-2465; (b) Grirrane, A.; Corma, A.; Garcia, H. *J. Catal.* **2009,** *264,* 138-144; (c) Zhang, Z.; Wang, F.; Wang, M.; Xu, S.; Chen, H.; Zhang, C.; Xu, J. *Green Chem.* **2014,** *16,* 2523-2527.

12. Naya, S.; Kimura, K.; Tada, H. *ACS Catal.* **2013,** *3,* 10-13.

13. Kawasaki, H.; Kumar, S.; Li, G.; Zeng, C.; Kauffman, D. R.; Yoshimoto, J.; Iwasaki, Y.; Jin, R. *Chem. Mater.* **2014,** *26,* 2777-2788.

14. (a) Becke, A. D. *Phys. Rev. A* **1988,** *38,* 3098–100; (b) Becke, A. D. *J. Chem. Phys.* **1993,** *98,* 5648–5652; (c) Burant, J. C.; Scuseria, G. E.; Frisch, M. J. *J. Chem. Phys.* **1996,** *105,* 8969–8972; (d) Frisch, M. J.; Trucks, G. W.; Schlegel, H. B.; Scuseria, G. E.; Robb, M. A.; Cheeseman, J. R.; Scalmani, G.; Barone, V.; Mennucci, B.; Petersson, G. A.; Nakatsuji, H.; Caricato, M.; Li, X.; Hratchian, H. P.; Izmaylov, A. F.; Bloino, J.; Zheng, G.; Sonnenberg, J. L.; Hada, M.; Ehara, M.; Toyota, K.; Fukuda, R.; Hasegawa, J.; Ishida, M.; Nakajima, T.; Honda, Y.; Kitao, O.; Nakai, H.; Vreven, T.; Montgomery, J. A., Jr.; Peralta, J. E.; Ogliaro, F.; Bearpark, M.; Heyd, J. J.; Brothers, E.; Kudin, K. N.; Staroverov, V. N.; Kobayashi, R.; Normand, J.; Raghavachari, K.; Rendell, A.; Burant, J. C.; Iyengar, S. S.; Tomasi, J.; Cossi, M.; Rega, N.; Millam, N. J.; Klene, M.; Knox, J. E.; Cross, J. B.; Bakken, V.; Adamo, C.; Jaramillo, J.; Gomperts, R.; Stratmann, R. E.; Yazyev, O.; Austin, A. J.; Cammi, R.; Pomelli, C.; Ochterski, J. W.; Martin, R. L.; Morokuma, K.; Zakrzewski, V. G.; Voth, G. A.; Salvador, P.; Dannenberg, J. J.; Dapprich, S.; Daniels, A. D.; Farkas, Ö.; Foresman, J. B.; Ortiz, J. V.; Cioslowski, J.; Fox, D. J. Gaussian, Inc., *Wallingford CT,* **2009**.

15. Hay, P. J.; Wadt, W. R. *J. Chem. Phys.* **1985,** *82,* 299–310.

16. Scalmani, G.; Frisch, M. J. *J. Chem. Phys.* **2010,** *132,* 114110–114115.

17. Qian, H.; Eckenhoff, W. T.; Bier, M. E.; Pintauer, T.; Jin, R. *Inorg. Chem.* **2011,** *50,* 10735-10739.

18. Jin, R.; Qian, H.; Wu, Z.; Zhu, Y.; Zhu, M.; Mohanty, A.; Garg, N. *J. Phys. Chem. Lett.* **2010,** *1,* 2903-2910.

19. Attar, S.; Bearden, W. H.; Alcock, N. W.; Alyea, E. C.; Nelson, J. H. *Inorg. Chem.* **1990,** *29,* 425-433.

20. Lang, X.; Ma, W.; Zhao, Y.; Chen, C.; Ji, H.; Zhao, J. *Chem. Eur. J.* **2012,** *18,* 2624-2631.

21. Lang, X.; Ji, H.; Chen, C.; Ma, W.; Zhao, J. *Angew Chem. Int. Ed.* **2011,** *50,* 3934-3937.

22. Antunes, C. S. A.; Bietti, M.; Salamone, M.; Scione, N. *J. Photochem. Photobiol., A* **2004,** *163,* 453-462.

23. Carp, O.; Huisman, C. L.; Reller, A. *Prog. Solid State Chem.* **2004,** *32,* 33-177.

24. Kogo, A.; Sakai, N.; Tatsuma, T. *Nanoscale* **2012,** *4,* 4217-4221.

25. Parker, J. F.; Weaver, J. E.; McCallum, F.; Fields-Zinna, C. A.; Murray, R. W. *Langmuir* **2010,** *26,* 13650-13654.

26. (a) Liu, C.; Abroshan, H.; Yan, C.; Li, G.; Haruta, M. *ACS Catal.* **2016,** *6,* 92-99; (b) Weare, W. W.; Reed, S. M.; Warner, M. G.; Hutchison, J. E. *J. Am. Chem. Soc.* **2000,** *122,* 12890-12891.

27. Roth, J. P.; Yoder, J. C.; Won, T. J.; Mayer, J. M. *Science* **2001,** *294,* 2524-2526.

28. Chen, Y.; Liu, C.; Abroshan, H.; Li, Z.; Wang, J.; Li, G.; Haruta, M. *J. Catal.* **2016,** *340*, 287-294.

29. Su, F.; Mathew, S. C.; Lipner, G.; Fu, X.; Antonietti, M.; Blechert, S.; Wang, X. *J. Am. Chem. Soc.* **2010,** *132*, 16299-16301.

30. (a) Furukawa, S.; Ohno, Y.; Shishido, T.; Teramura, K.; Tanaka, T. *ACS Catal.* **2011,** *1*, 1150-1153; (b) Su, F.; Mathew, S. C.; Mohlmann, L.; Antonietti, M.; Wang, X.; Blechert, S. *Angew Chem. Int. Ed.* **2011,** *50*, 657-660; (c) Raza, F.; Park, J. H.; Lee, H.-R.; Kim, H.-I.; Jeon, S.-J.; Kim, J.-H. *ACS Catal.* **2016,** *6*, 2754-2759.

Table of contents